Measurements of Proton Total Reaction Cross Sections for Lithium-6, Lithium-7, natural Boron, Nitrogen-14, Neon-20, Argon-40 and natural Titanium between 20 and 50 MeV.

by

TAWFIK N. NASR

May, 1977

A thesis submitted to the Faculty of Graduate Studies of the University of Manitoba in partial fulfilment of the requirements for the degree of Master of Science.

MEASUREMENTS OF PROTON TOTAL REACTION CROSS SECTIONS FOR LITHIUM-6, LITHIUM-7, NATURAL BORON, NITROGEN-14, NEON-20, ARGON-40 AND NATURAL TITANIUM BETWEEN 20 and 50 MeV.

BY

TAWFIK N. NASR

A dissertation submitted to the Faculty of Graduate Studies of the University of Manitoba in partial fulfillment of the requirements of the degree of

MASTER OF SCIENCE

ABSTRACT

Using a variation of the standard attenuation technique and a tightly collimated and momentum analyzed proton beam, total reaction cross sections, σ_R, have been measured for ^{6}Li, ^{7}Li, B, ^{14}N, ^{20}Ne, ^{40}Ar and Ti over the energy range 20 to 50 MeV at the University of Manitoba Cyclotron Laboratory. The ^{6}Li, ^{14}N, ^{20}Ne, ^{40}Ar and Ti total reaction cross sections are compared with optical model predictions obtained from analyses of elastic scattering differential cross section and polarisation data for these elements in the energy range under study. The B data are compared with σ_R values of the nearby elements ^{9}Be and ^{12}C. The measured total reaction cross sections are compared with predictions of the opaque nucleus model. The Ti cross sections are presented along with the existing reaction data available in the literature.

ACKNOWLEDGMENTS

I would like to express my gratitude to my supervisor Dr. W.T.H. van Oers for his fruitful suggestions and encouragement which greatly stimulated my interest in this work. I wish also to express my thanks to Dr. A.M. Sourkes for many useful discussions. I am indebted to Dr. R.F. Carlson, Dr. A.J. Cox and Dr. D.J. Margaziotis for their help in setup of the experiments. Finally, the help and cooperation of the University of Manitoba Cyclotron Laboratory technical staff are well acknowledged.

My thanks are due to my wife Tahany for her patience and understanding during the preparation of this thesis.

TABLE of CONTENTS

LIST of FIGURES

CHAPTER 1

1.1 Introduction

Total reaction cross section (σ_R) data provide an important constraint on the imaginary phases obtained from phase shift analyses of light nucleus elastic scattering data. Recently, nucleon-deuteron disintegration cross sections have been calculated using the Faddeev formalism (Sl71). These calculated values were systematically about 10% lower than measurements of this quantity (Ca73), suggesting a possible change in the nuclear interaction information to be used in the calculations.

For heavier nuclides σ_R values determine, to a large extent, the phenomenological imaginary potential in the optical model (Pe63). Proton elastic scattering and polarisation data in the low to intermediate energy range for medium and certain light weight nuclides have provided a great deal of information about the nucleus through use of the nuclear optical model (Ho67). This model assumes a spherical potential with geometrical and dynamical potential parameters representing the nucleon-nucleus interaction. Detailed optical model studies (Fr67,Be69) have indicated that the dynamical parameters vary with energy in a systematic way. A study of the

form of this variation requires as complete a set of nuclear scattering measurements as possible.

Except for two recent studies (So74,Ca75) most total reaction cross section work has been concerned with the behaviour of the cross section as a function of mass number for a single incident energy (Wi63,Ma64,Tu64,Po65, Ki66,Me71). The latter studies have shown that at a given energy the data are well represented by a relation of the form

$$\sigma_R = \pi \left(r_0 A^{1/3} + \lambda \right)^2 \qquad (1)$$

where r_0 is the radius parameter and λ is the reduced wavelength for the relative motion of the projectile and target. It should be noted that, since r_0 is not entirely energy independent, the above expression does not necessarily reproduce the energy dependence of the total reaction cross section for a particular nucleus over a range of energies with a unique r_0.

The present work examines the total reaction cross section of the nuclides ^{6}Li , ^{7}Li , B , ^{14}N , ^{20}Ne , ^{40}Ar , and Ti over the energy range 20 to 50 MeV through direct measurement and makes comparison with measurements of neighbouring elements and with optical model calculations of the total reaction cross section.

1.2 The optical model

The nucleon-nucleus interaction can be determined by two approaches, i.e, either theoretically by summing the nucleon-nucleon interactions, or phenomenologically by representing the nucleon-nucleus interaction as a sum of central and spin-orbit terms, with the appropriate radial dependences. The first approach faces unresolved mathematical difficulties in solving the many-body problem; however this difficulty can be overcome at higher energies (>100 MeV) where the impulse approximation is valid. In the second approach the experimentally measured elastic scattering differential cross section, polarisation , and total reaction cross section data are fitted by a potential of assumed form. A best fit to the data is obtained by varying the parameters of the potential. The disadvantage of this approach is that there is no unique set of parameters which produce the best fit to the experimental data.

1.3 The optical potential

The basic assumption of the optical model is that the nucleon-nucleus interaction can be represented by a one-body potential between the nucleon and the nucleus. A complex potential accounts for the elastic scattering

as well as for absorption of particles from the incident beam. This complex potential is referred to as the optical potential because of the analogy of the elastic and inelastic interaction between nucleons and nuclei with the reflection and absorption of light by a medium with a complex refractive index. The optical potential can be written as

$$U(r) = -V f(x_0) - iW f(x_i) \qquad (2)$$

where V and W are the depth of the real and imaginary parts respectively, $x_i = \frac{r - r_i A^{1/3}}{a_i}$, $f(x_i)$ is a radial form factor, r is the distance between the nucleon and the center of mass of nucleus, a_i and r_i are the diffuseness and radius parameters and A is the mass number of the target nucleus.

The form factors $f(x_i)$ are expected to satisfy two important features. Firstly, to fall exponentially with increasing radial distance, since this is a feature of the nucleon-nucleon interaction and, secondly, to be uniform inside the nucleus, since nuclear forces are known to saturate, that is to say a nucleon is acted upon by the immediately adjacent nucleons only and thus experiences no appreciable resultant force. The two requirements are represented by the Woods-Saxon form factor (Wo54) given by

$$f(x_i) = (1 + e^{x_i})^{-1} \qquad (3)$$

For protons one must add a Coulomb potential to the nuclear potential given in equation (2). The Coulomb potential can be represented accurately enough by a potential due to a uniformly charged sphere which has the form

$$V_c(r) = \frac{Ze^2}{2R}\left[3 - \left(\frac{r}{R}\right)^2\right] \quad \text{for} \quad r < R$$

$$= \frac{Ze^2}{r} \quad \text{for} \quad r > R$$

where R is the Coulomb radius $R = r_o A^{1/3}$, and r_o is the radius parameter.

By introducing a surface absorption term of the form $4 i W_I a_I \frac{d}{dr} f(x_I)$ to the volume absorption term (imaginary part of equation (2)) a better fit to the experimental data is obtained. The reason for choosing this term is that the absorption of the incident nucleons by the target nucleus is opposed by the Pauli exclusion principle inside the nucleus where most shells are filled. So we expect the absorption process to take place preferentially at the surface of the nucleus, in particular at lower energies where the exclusion principle is more effective.

The early optical model calculations, made with central forces alone, were found to give good fits to the

differential elastic scattering cross-sections, but they predicted no polarisation. To account for the polarisation a spin-orbit term of the form

$$(V_{so} + iW_{so}) \frac{4}{r} \left[\frac{d}{dr} f(x_{so}) \right] (\bar{S}.\bar{L}) \qquad (4)$$

was introduced (Fe54) into the optical potential. By analogy with the shell model potential the spin-orbit term is chosen to be of the Thomas form.

Thus the optical model potential can be written as

$$U(r) = V_c(r) - V f(x_0) - iW f(x_i) + i4W_i a_i \frac{d}{dr} f(x_i) + (V_{so} + iW_{so})(\bar{S}.\bar{L}) \frac{4}{r} \frac{d}{dr} f(x_{so}) \qquad (5)$$

This potential has therefore twelve adjustable parameters; seven geometrical parameters, namely r_c, r_o, a_o, r_i, a_i, r_{so}, a_{so} and five dynamical parameters, namely V, W, W_i, V_{so}, W_{so}. These twelve parameters can be varied to obtain the best fit to the experimental differential elastic cross section, polarisation and total reaction cross sections by minimizing the quantity

$$\chi^2 = \sum_{i=1}^{N_\sigma} \left[\frac{\left(\frac{d\sigma(\theta_i)}{d\Omega}\right)_{th} - \left(\frac{d\sigma(\theta_i)}{d\Omega}\right)_{exp}}{\Delta\left(\frac{d\sigma(\theta_i)}{d\Omega}\right)} \right]^2 + \sum_{j=1}^{N_P} \left[\frac{P_{th}(\theta_j) - P_{exp}(\theta_j)}{\Delta P(\theta_j)} \right]^2 + \left[\frac{\sigma_R^{th} - \sigma_R^{exp}}{\Delta\sigma_R} \right]^2$$

where N_σ and N_P are the numbers of experimental differential cross-sections and polarisations respectively. The

quantities $\left(\frac{d\sigma(\theta_i)}{d\Omega}\right)_{th}$ and $\left(\frac{d\sigma(\theta_i)}{d\Omega}\right)_{exp}$ are the theoretical and experimental differential cross section at the scattering angle θ_i , while $\Delta\left(\frac{d\sigma(\theta_i)}{d\Omega}\right)$ is the experimental error of the differential cross-section at θ_i. Similarly, $P_{th}(\theta_j)$ and $P_{exp}(\theta_j)$ are the theoretical and experimental polarisation at the scattering angle θ_j, while $\Delta P(\theta_j)$ is the experimental error of the polarisation at θ_j. σ_R^{th} and σ_R^{exp} are the theoretical and experimental values of the total reaction cross section and $\Delta\sigma_R$ is the experimental error.

CHAPTER 2

2.1 Cyclotron and Beam Line

The experiment was performed by using the external proton beam from the University of Manitoba sector-focussed cyclotron. A beam of negative hydrogen ions is injected axially into the center of the cyclotron at 11 keV. An electrostatic mirror is used to deflect these ions into the median plane where they are accelerated by the 28 kV rf voltage. Extraction is achieved by stripping the two electrons from the negative hydrogen ions using a thin aluminum foil. The magnetic force on the hydrogen ions thereby reverses, sweeping the beam out of the cyclotron field. By changing the radius and the angle of the stripping foil position and by using a small external magnetic field from the combination magnet it is possible to extract proton beams of energies between 20 and 50 MeV.

The layout of the experimental beam facility is shown in Fig.1. The proton beam leaving the cyclotron was centered with respect to the axis of the beam line by using the combination magnet and varying the stripping foil angle. Steering magnets St1 and St2 were also used if necessary. The doublet of quadrupole lenses Q1-Q2

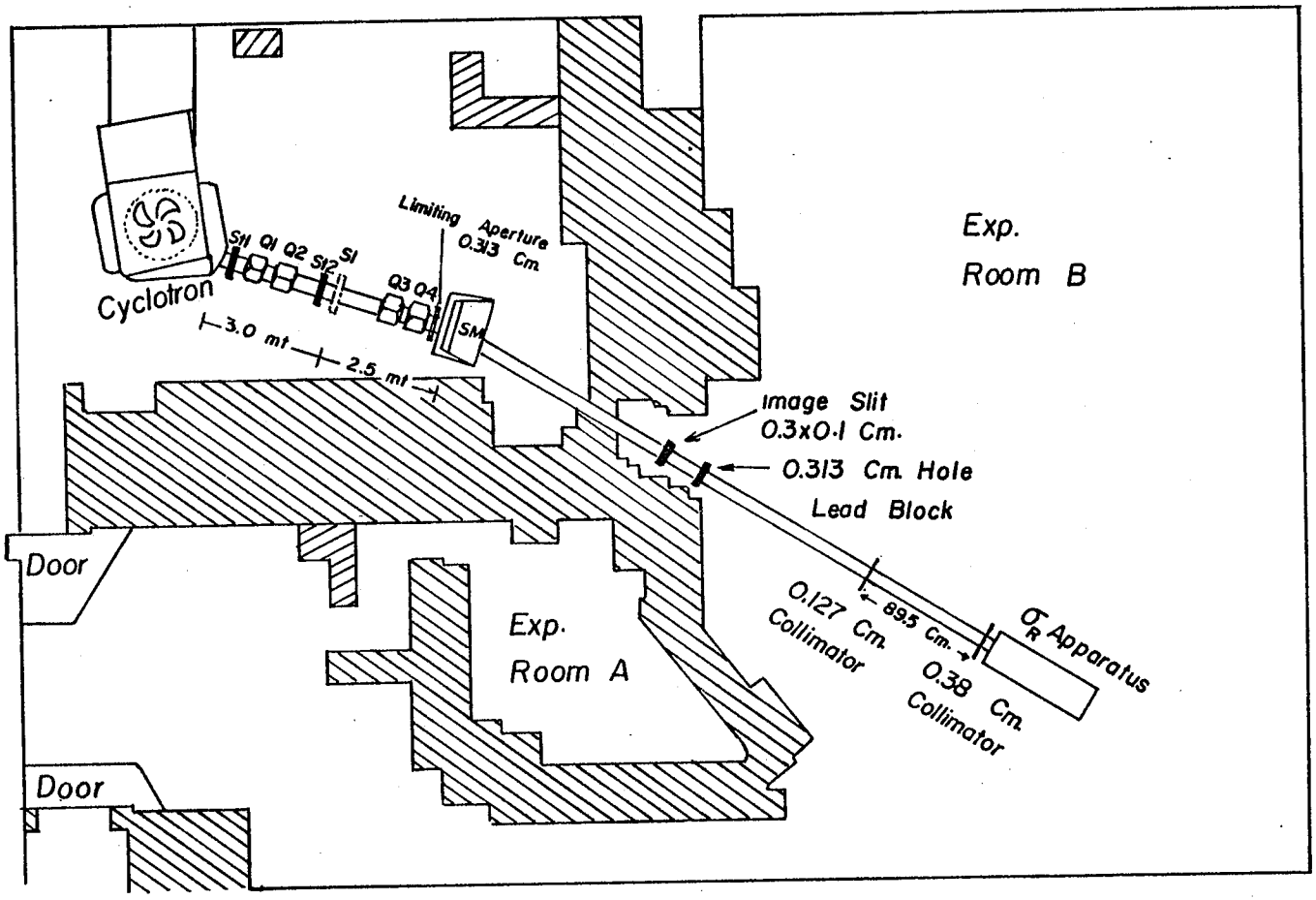

Cyclotron Beam Line Layout

Fig. 1

produced a horizontal and vertical waist at the position of the first slit box (S1). The switching magnet deflected the beam into the 15° right beam line to the total reaction cross section apparatus. A limiting aperture (a carbon block with 0.313 cm diameter hole) was located at the entrance to the switching magnet, while a lead block with 0.313 cm diameter hole and placed farther downstream, as shown in Fig.1, served as a neutron attenuator. Quadrupole Q3 was turned off during the experiment while Q4 was used to retract the focal plane of the bending magnet onto the location of the image slits (with an apertures 0.3 cm high by 0.1 cm wide). The size and direction of the beam were further defined by a 0.127 cm diameter circular collimator located upstream from the σ_R apparatus

2.2 Apparatus

The total reaction cross section apparatus used in the experiment is shown schematically in Fig.2. This apparatus consists of an evacuated tube fitted with a beam defining collimator mentioned above. The antiscattering baffle, which is a brass disc with a 0.38 cm diameter hole, is located 89.5 cm downstream from the collimator and is used to remove protons which are scattered by the

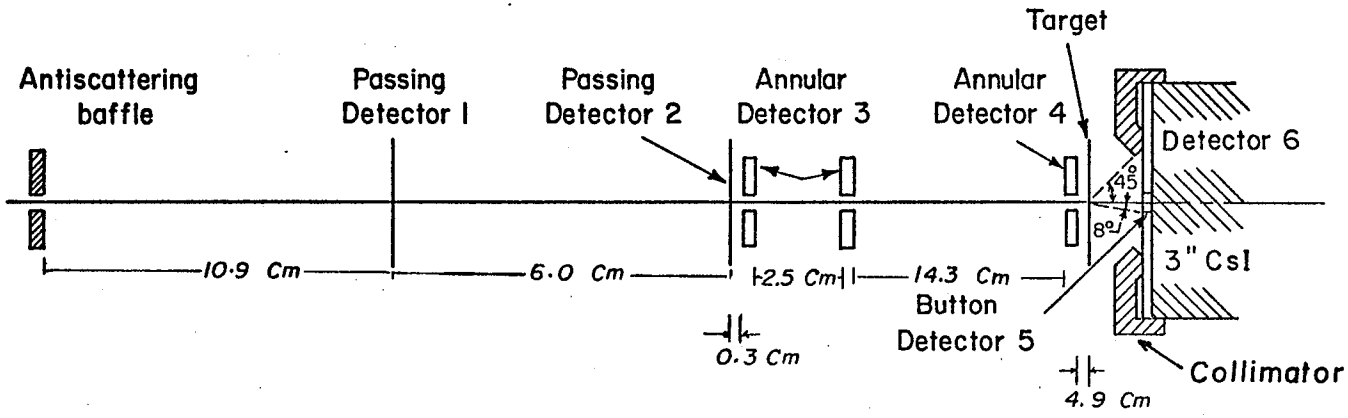

Schematic diagram of the total reaction cross section apparatus

Fig. 2

edge of the collimator.

The passing detectors 1 and 2 are two plastic scintillators separated by a distance of about 6.0 cm and constructed from a thin NE-102 sheet 1 cm in diameter and 0.013 cm thick. Each of the scintillators is mounted in a cylindrical tube whose inner surface is coated with white reflecting paint. One end of the tube is closed while the other end is open for viewing by a photomultiplier tube through a lucite window, which also forms a vacuum seal. The beam enters and leaves the cylindrical tube through 1.3 cm diameter holes on the sides covered with aluminized mylar (0.0006 cm thick). Scintillator 1 is located at 10.9 cm from the antiscattering baffle and mounted at the end of a post at the center of the cylindrical tube, while scintillator 2 is mounted on a post located as close as possible to the beam exit hole in the tube. The distance between passing detector 2 and the first scintillator disc of annular detector 3 is about 0.3 cm.

The annular detector 3 consists of a pair of plastic scintillators with a hole at the center of each scintillator. The first and second holes are respectively 0.236 cm and 0.305 cm in diameter. Each scintillator is mounted on a lucite holder covered with aluminized mylar and slides into a cavity in the apparatus. These

scintillators are held perpendicularly to the beam direction with their central holes concentric with the beam (The distance between the two scintillator discs of annular detector 3 is 2.5 cm and the second scintillator disc of annular detector 3 is at 19.2 cm from the solid target location (See Fig.2)). Each cavity is vacuum sealed with a lucite disc and both ends are viewed by photomultipliers. Annular detector 4 is the same as annular detector 3, with the exception that it has only one scintillator disc with a center hole of 0.368 cm diameter and is located at 4.9 cm from the position of the solid target.

Solid targets are mounted on a target wheel which is 10.3 cm diameter; the wheel can accommodate 8 targets. The wheel is turned by an electric motor which is fitted with a synchro-readout, allowing the target to be positioned remotely to an accuracy of 0.013 cm. In case of gaseous targets the target wheel is replaced by a gas cell which is a 3 cm long brass cylinder with nickel entrance and exit foils 0.0025 and 0.0076 cm thick, respectively, (Fig.3).

Immediately following the target is a collimator which, for solid targets, defines a cone of opening angle $\pm 45^{\circ}$ for the acceptance of scattered protons by the telescope system, detectors 5 and 6. In the case of a

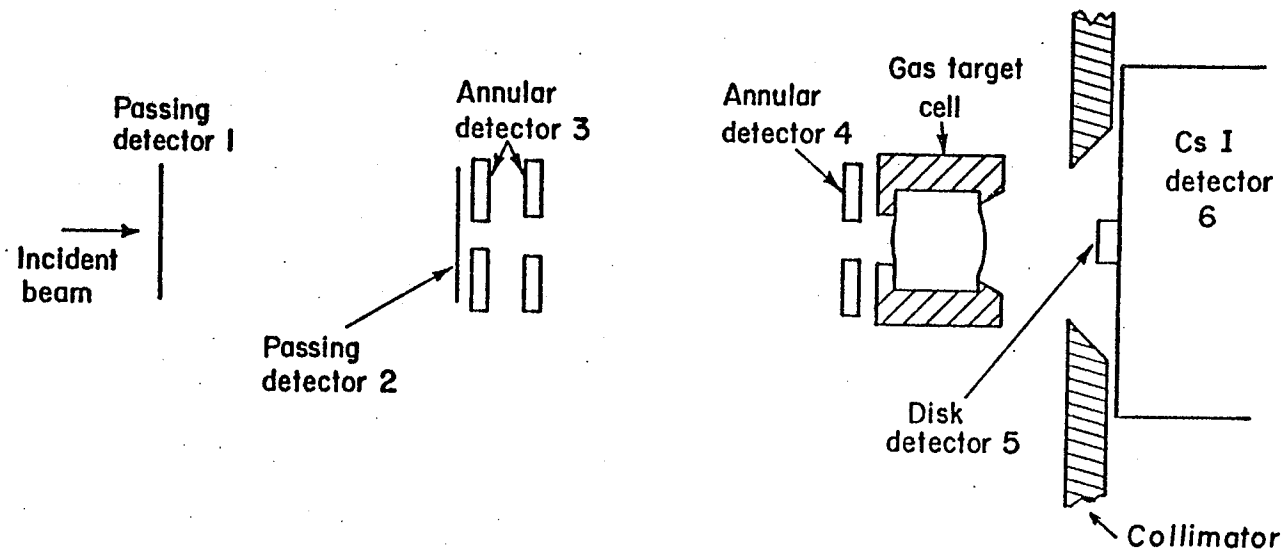
Passing
detector 1
Incident
beam
Annular
detector 3
Passing
detector 2
Annular
detector 4
Gas target
cell
Cs I
detector
6
Disk
detector 5
Collimator

Fig. 3

gas target the acceptance angle depends on the point in the cell from which the proton was scattered.

Detectors 5 and 6 form the energy analyzing system. Detector 5 is a plastic scintillator disc of 0.635 cm diameter and 0.102 cm thickness embedded in a flat lucite light pipe 0.157 cm thick which passes out through slots in the target block for viewing by two photomultiplier tubes. Each photomultiplier tube views one end of the light pipe through a lucite vacuum sealing window. Detector 5 subtends a cone of half-angle 8° with respect to the center of the solid target. The stopping detector 6 is a cesium iodide crystal 8.9 cm diameter and 3.1 cm thick coupled to a photomultiplier tube through a vacuum sealing lucite light pipe. This detector is located directly behind detector 5 (Ca75b).

2.3 Electronics

2.3.1 Logic operation

An I_o pulse, which represents a proper incident proton event, is generated whenever passing detectors 1 and 2 produce signals in coincidence in the absence of pulses from annular detectors 3 and 4 (See Fig.4). After an I_o event is recorded an electronic circuit is operated to determine whether or not the incident proton has been

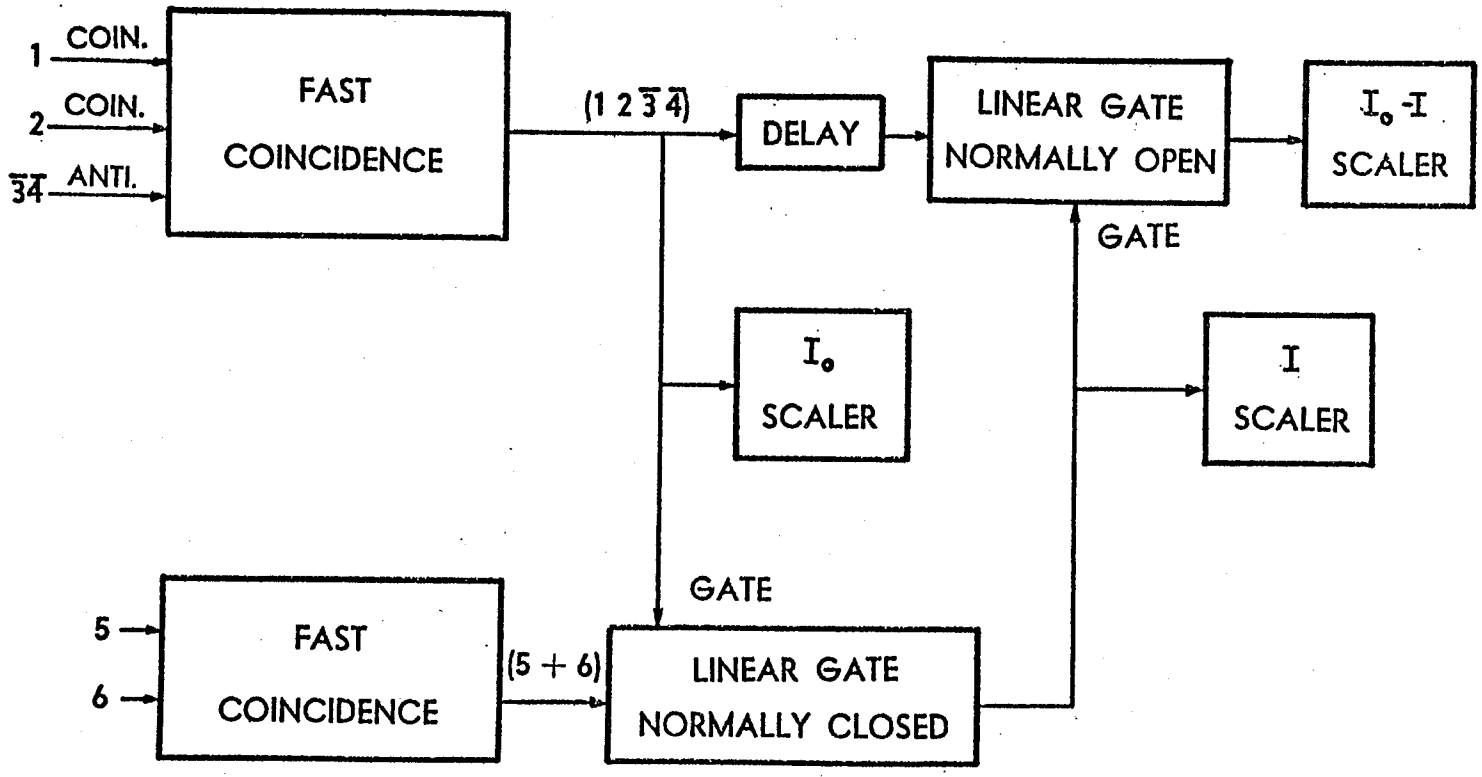
1 COIN.
2 COIN.
$\overline{34}$ ANTI.
FAST COINCIDENCE
(1 2 $\overline{3}$ $\overline{4}$)
DELAY
LINEAR GATE NORMALLY OPEN
$I_o - I$ SCALER
GATE
I_o SCALER
I SCALER
GATE
5
6
FAST COINCIDENCE
(5 + 6)
LINEAR GATE NORMALLY CLOSED

Fig. 4

removed from the beam by the target. If this proton is not removed an I event is recorded. The two pulses I and I_o are combined in a logic circuit to produce (I_o-I), which represents the number of protons removed from the beam by the target. This number can be measured directly and is related to the total reaction cross section. The I_o pulse is denoted $(12\bar{3}\bar{4})$ and represents a proton which has passed unscattered through detectors 1 and 2 and has passed through the central portion of the annular detectors 3 and 4. The I_o pulse is split into two branches. One branch is used to open a normally closed linear gate, while the other branch goes to the signal input of a normally open linear gate (Fig.4). If the incident proton has not undergone a nuclear reaction in the target but has scattered in a forward cone of half-angle equal to the maximum acceptance angle of detector 6, a pulse is generated by an OR circuit and is denoted (5+6). This (5+6) pulse passes through the linear gate opened by the I_o pulse and registers as an I event and closes the linear gate which is normally open and prevents the delayed I_o pulse from passing through the gate (and registering as an attenuation event). On the other hand, if the proton has undergone a nuclear reaction in the target no (5+6) signal is produced and the delayed I_o pulse passes through the normally open gate and registers as an attenuation

(I_o-I) event.

2.3.2 The Electronics Diagram

The fast pulses from the anodes of detectors 1 and 2, preamplified in the experimental area, are then fed to fast discriminators. An additional discriminator is used for detector 2 to obtain a short pulse for the pile-up gate. The output of the discriminators are fed to the input of a five-fold logic unit operated in two-fold coincidence mode. The signals from the anodes of the two photomultipliers viewing annular detector 3 are summed and amplified in the experimental area. The same applies to annular detector 4. These signals are fed into discriminators and then to a fan-in unit, the output of which is connected to the lo-veto input of the pile-up gate, which produces an inhibit pulse whenever a pulse is received from the fan-in unit. The output of the five-fold unit is $12\bar{3}\bar{4}$. The dynode signals of detectors 5 and 6 are preamplified and amplified in the experimental area. In the control room these signals are fed into integral discriminators whose negative outputs feed into a five-fold logic unit which operates as an OR gate. The output of this gate is (5+6).

The positive output of the integral discriminator of

detector 5 is delayed and fed into a coincidence unit. The unit produces an output if it receives pulses from detector 5, detector 6 and the I_o scaler within 8 μsec of each other. The number of such events is recorded by the E+B scaler.

The positive output of the integral discriminator of detector 6 is delayed and then sent to a coincidence unit. This unit produces an output if the I_o signal is in coincidence with the signal from detector 6 and in anticoincidence with the $\bar{B}$ signal from detector 5. The output of this coincidence unit is fed into the E-$\bar{B}$ scaler.

To make sure that the normally closed gate, which is opened by a $12\bar{3}\bar{4}$ pulse, remains open long enough for the associated (5+6) pulse (i.e I pulse), if any, to pass through, and that the normally open gate, which is closed by the I pulse, remains shut long enough to block the I_o pulse completely, a pile-up circuit was introduced in the electronic system. This circuit produces an inhibit pulse whenever it receives a pair of input pulses less than a preset time apart. The pile-up inhibit pulse remains as long as pairs are received within the the pile-up resolving time, which can be selected. Usually a resolving time of 8 μsec was chosen.

The output pulse of detector 6 linear amplifier is

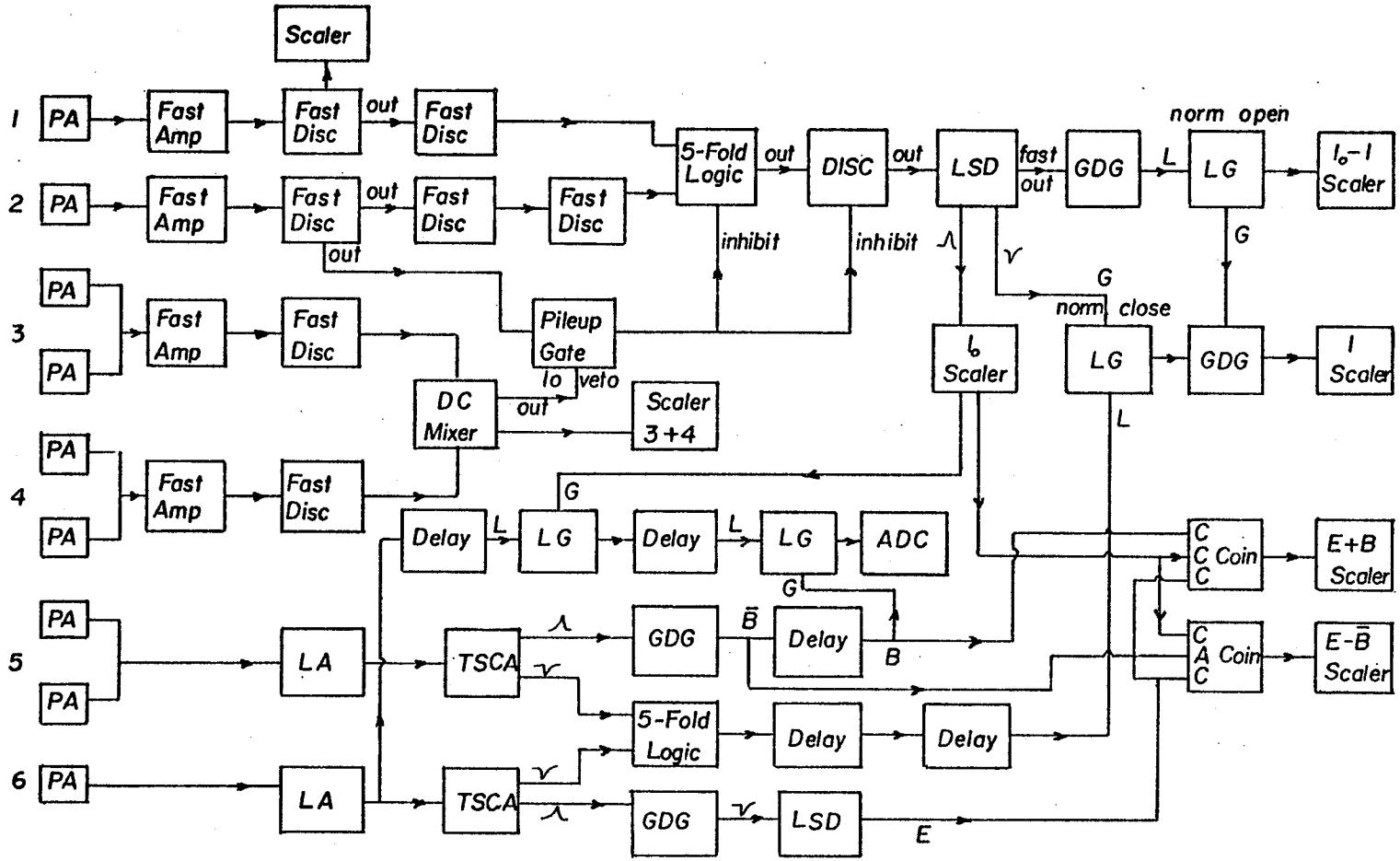

The Electronics Diagram

Fig. 5